frontiers in Chemistry

ORIGINAL RESEARCH
published: 16 April 2020
doi: 10.3389/fchem.2020.00279

Meroterpenoids With Protein Tyrosine Phosphatase 1B Inhibitory Activities From the Fruiting Bodies of *Ganoderma ahmadii*

Jiaocen Guo[1,2†], Fandong Kong[1†], Qingyun Ma[1], Qingyi Xie[1], Renshuai Zhang[3], Haofu Dai[1], Yougen Wu[2] and Youxing Zhao[1*]*

[1] Hainan Key Laboratory for Research and Development of Natural Product From Li Folk Medicine, Institute of Tropical Bioscience and Biotechnology, Chinese Academy of Tropical Agriculture Sciences, Haikou, China, [2] College of Horticulture, Hainan University, Haikou, China, [3] Qingdao Cancer Institute, The Affiliated Hospital of Qingdao University, Qingdao, China

OPEN ACCESS

Edited by:
Prasat Kittakoop, Chulabhorn Graduate Institute, Thailand

Reviewed by:
Christophe Salome, SpiroChem AG, Switzerland
Florenci Vicent González, University of Jaume I, Spain

***Correspondence:**
Yougen Wu
wygeng2003@163.com
Youxing Zhao
zhaoyouxing@itbb.org.cn

[†] These authors have contributed equally to this work

Specialty section:
This article was submitted to Organic Chemistry, a section of the journal Frontiers in Chemistry

Received: 31 December 2019
Accepted: 23 March 2020
Published: 16 April 2020

Citation:
Guo J, Kong F, Ma Q, Xie Q, Zhang R, Dai H, Wu Y and Zhao Y (2020) Meroterpenoids With Protein Tyrosine Phosphatase 1B Inhibitory Activities From the Fruiting Bodies of Ganoderma ahmadii. Front. Chem. 8:279. doi: 10.3389/fchem.2020.00279

Ganoderma fungi have long been used as functional foods and traditional medicines in Asian countries. *Ganoderma ahmadii* is one of the main species of *Ganoderma* fungi distributed in Hainan province of China, the fruiting bodies of which have been used in folk to lower blood sugar for a long time. A chemical investigation of the fruiting bodies of *Ganoderma ahmadii* led to the isolation of seven new meroterpenoids, named ganoduriporols F-L **(1–7)**. The chemical structures of the compounds were elucidated by spectroscopic data including HRESIMS and 2D NMR. Compounds **5–7** represent the first examples of ganoduriporol-type meroterpenoids bearing oxepane rings in their skeletons. Compounds **1–4** showed inhibitory activity against protein tyrosine phosphatase 1B (PTP1B) comparable to the positive control Na_3VO_4, with IC_{50} values of 17, 20, 19, and 23 μM, respectively.

Keywords: *Ganoderma ahmadii*, meroterpenoid, spectroscopic, PTP1B, cytotoxicity

INTRODUCTION

Ganoderma fungi have been widely used as functional foods and traditional medicines, which have provided more efficient means for human health care, nutrition, medical care in China (Ma et al., 2019). It has been regarded as one of the most important medicinal fungi for preventing and treating various human diseases in Asian countries (Paterson, 2006). Previous studies have showed that the bioactive constituents of these fungi are mainly triterpenoids (Baby et al., 2015), polysaccharides (Wang et al., 2014), alkaloids (Zhao et al., 2015), and meroterpenoids (Yan et al., 2013) etc. These compounds with diverse structures displayed various biological effects, such as anti-tumor (Fu et al., 2019), anti-inflammatory (Lu et al., 2019), anti-diabetes (Wang et al., 2017), immunomodulation (Ji et al., 2007), and anti-oxidation activities (Qiu et al., 2016). Recently, a great deal of work on *Ganoderma* fungi have found that some constituents extracted from *Ganoderma* can promote the release of serum insulin and decrease the plasma glucose concentration *in vivo* (Huang et al., 2010; Li et al., 2017; Zhao and He, 2018).

Recent studies on the pathological mechanism revealed that type 2 diabetes has a close relationship with the protein tyrosine phosphatase family, which plays an important role in the negative regulator of insulin signaling by dephosphorylating the tyrosine residues of proteins (Tamrakar et al., 2014). PTP1B is an important member of the protein tyrosine phosphatase family

and is responsible for insulin signaling pathway (Wang et al., 2015). Insulin resistance caused by expression of PTP1B as well as dephosphorylation of its target is one of the main causes of type 2 diabetes (Cai et al., 2015). Thus, PTP1B has been identified as a target for research and development of new drugs for the treatment of type 2 diabetes, and PTP1B inhibitors are potential lead compounds for such new drugs (Teng et al., 2011).

Ganoderma ahmadii is mainly distributed in Hainan, Yunnan, and Guizhou provinces in China (Wu and Dai, 2005), which have been used in folk medicine to lower blood sugar for a long time. As our ongoing search for bioactive constituents from the genus *Ganoderma* (Zhang et al., 2015; Huang et al., 2016, 2017), the bioactive constituents from *G. ahmadii* was studied, which led to the isolation of three new meroterpenoids with PTP1B inhibitory activity (Guo et al., 2019). A continuous research resulted in the isolation of another seven new meroterpenoids, named ganoduriporols F-L (**1–7**). Herein, the isolation, structural characterization, and PTP1B inhibitory activities of these compounds are reported.

MATERIALS AND METHODS

General Experimental Procedures

The NMR spectra were recorded on a Bruker AV-500 spectrometer (Bruker, Bremen, Germany), and using tetramethylsilane (TMS) as an internal standard. Chemical shifts (δ) were expressed in ppm with reference to TMS. High Resolution Electrospray Ionization Mass Spectroscopy (HRESIMS) data were acquired using a mass spectrometer API QSTAR Pulsar (Bruker, Bremen, Germany). Optical rotations were measured using a JASCO P-1020 digital polarimeter. UV spectra were obtained with a Beckman DU 640 spectrophotometer. IR spectra were recorded on with a Shimadzu UV2550 spectrophotometer (Japan). Semipreparative high-performance liquid chromatography (HPLC) equipped with octadecyl silane (ODS) column (COSMOSIL-pack ODS-A, 10 × 250 nm, 5 μm, 4 ml/min) and phenyl (PH) column (COSMOSIL-pack ph, 10 × 250 nm, 5 μm, 4 ml/min) were used to isolate compounds. Silica gel (200-300 mesh; Qingdao Marine Chemical Inc., Qingdao, China) and Sephadex LH-20 (40–70 μm; Merck, Darmstadt, Germany) were used for column chromatography. Thin-layer chromatography (TLC) was carried out with precoated Si gel plates.

Plant Material

The *Ganoderma ahmadii* were collected in June 2017 Qiongzhong County, Hainan Province, China. The fungal material was identified by Prof. Zeng Nian-Kai (Hainan Medical University, China). The certified specimen (No.011-ZLZ) was deposited in the Institute of Tropical Bioscience and Biotechnology, Chinese Academy of Tropical Agricultural Sciences.

Extraction and Isolation

The dried and powdered fruiting bodies of *G. ahmadii* (5.0 kg) were extracted with 95% ethanol three times at room temperature. After filtration and evaporation, a gummy residue was obtained, which was taken up in H_2O and with petroleum ether, ethyl acetate (EtOAc), and n-butanol. The EtOAc extract (55.0 g) was subjected to column chromatography (CC) on silica gel with gradient elution (petroleum ether-EtOAc, 8:1–1:2), which yielded seven fractions (Fr.1–Fr.7). Fr.6 (5.0 g) was further separated using an octadecyl silane silica gel column and eluted with gradient solvent of MeOH-H_2O (30–100%) to give seven fractions (Fr.6.1–Fr.6.7), Fr.6.5 (116.0 mg) was purified by semipreparative HPLC [42% MeCN/H_2O, containing 0.1% trifluoroacetic acid (TFA)] to afford compound **2** (t_R 15.0 min; 3.5 mg). Fr.6.6 (140.0 mg) was further purified using semipreparative HPLC (70% MeOH/H_2O, containing 0.1% TFA) to give compound **4** (t_R 12.2 min; 3.0 mg). Fr.7 (6.0 g) was subjected to CC on an ODS elution with MeOH-H_2O (20–100%) to give nine fractions (Fr.7.1–Fr.7.9). Fr.7.1 (2.2 g) was subjected to Sephadex LH-20 eluting with $CHCI_3$-MeOH-petroleum ether (1:1:1) yielded three sub-fractions (Fr.7.1.1–7.1.3) based on TLC. Fr.7.1.2 (87.0 mg) was further purified by semipreparative HPLC (45% MeCN/H_2O; containing 0.1% TFA) to afford compound **3** (t_R 7.8 min; 3.0 mg). Fr.7.1.3 (70.0 mg) was subjected to semipreparative HPLC (65% MeOH/H_2O; containing 0.1% TFA) to afford compound **6** (t_R 32.0 min; 3.0 mg). Fr.7.2 (150.0 mg) was further purified by semipreparative HPLC (45% MeCN/H_2O; containing 0.1% TFA) to afford compounds **7** (t_R 20.7 min; 3.3 mg) and **5** (t_R 22.2 min; 3.0 mg). Fr.7.7 (1.5 g) was subjected to Sephadex LH-20 (MeOH) to afford five fractions (Fr.7.7.1–Fr.7.7.5), in which Fr.7.7.4 (80.0 mg) was further prepared by semipreparative HPLC (72% MeOH/H_2O, containing 0.1% TFA) to produce compound **1** (t_R 14.2 min; 3.5 mg).

Characterization of Compounds 1–7

Ganoduriporol F (**1**): yellow oil; UV (MeOH) λ max (log ε) 307 (4.4), 224 (4.0) nm; IR (KBr) ν_{max} (cm^{-1}): 3436, 2925, 2851, 1630, 1388, 1168 (**Figure S9**); ^1H and ^{13}C NMR data, see **Tables 1**, **2**; HRESIMS *m/z* 559.1938 $[M + Na]^+$ (calcd for $C_{30}H_{32}NaO_9$, 559.1939).

Ganoduriporol G (**2**): yellow oil; $[\alpha]_D^{25}$ +12 (*c* 0.1, MeOH); UV (MeOH) λ $_{max}$ (log ε) 328 (4.1), 288 (3.8) nm; IR (KBr) ν_{max} (cm^{-1}): 3414, 2927, 2859, 1610, 1474, 1263, 1195 (**Figure S18**); ^1H and ^{13}C NMR data, see **Tables 1**, **2**; HRESIMS *m/z* 577.2046 $[M + Na]^+$ (calcd for $C_{30}H_{34}NaO_{10}$, 577.2044).

Ganoduriporol H (**3**): yellow oil; $[\alpha]_D^{25}$ +10 (*c* 0.1, MeOH); UV (MeOH) λ $_{max}$ (log ε) 311 (4.3), 259 (4.0), 206 (4.8) nm; IR (KBr) ν_{max} (cm^{-1}): 3418, 2927, 2851, 1688, 1606, 1511, 1389, 1170 (**Figure S27**); ^1H and ^{13}C NMR data, see **Tables 1**, **2**; HRESIMS *m/z* 603.2212 $[M + Na]^+$ (calcd for $C_{32}H_{36}NaO_{10}$, 603.2201).

Ganoduriporol I (**4**): yellow oil; $[\alpha]_D^{25}$ +17 (*c* 0.1, MeOH); UV (MeOH) λ $_{max}$ (log ε) 292 (4.1), 247 (3.8) nm; IR (KBr) ν_{max} (cm^{-1}): 3435, 2926, 2851, 1685, 1603, 1449, 1268, 1169 (**Figure S36**); ^1H and ^{13}C NMR data, see **Tables 1**, **2**; HRESIMS *m/z* 603.2169 $[M + Na]^+$ (calcd for $C_{32}H_{36}NaO_{10}$, 603.2201).

Ganoduriporol J (**5**): yellow oil; $[\alpha]_D^{25}$ +8 (*c* 0.1, MeOH); UV (MeOH) λ $_{max}$ (log ε) 299 (4.2), 264 (4.0), 225 (4.5) nm; IR (KBr) ν_{max} (cm^{-1}): 3418, 2927, 2855, 1691, 1604, 1512, 1271, 1170 (**Figure S45**); ^1H and ^{13}C NMR data, see **Tables 1**, **2**; HRESIMS *m/z* 561.2065 $[M + Na]^+$ (calcd for $C_{30}H_{34}NaO_9$, 561.2095).

TABLE 1 | ^{13}C NMR (125 MHz) Data of Compounds **1–7** in CD_3OD (δ in ppm).

NO.	1	2	3	4	5	6	7
1	157.1, C	157.2, C	156.6, C	157.2, C	156.6, C	156.6, C	156.6, C
2	121.4, C	121.3, C	120.4, C	121.3, C	121.0, C	121.1, C	120.9, C
3	115.8, CH	115.8, CH	115.7, CH	115.8, CH	116.0, CH	116.1, CH	115.9, CH
4	150.7, C	150.8, C	150.7, C	150.8, C	150.6, C	150.5, C	150.6, C
5	126.7, CH	126.7, CH	125.9, CH	126.7, CH	126.0, CH	126.0, CH	126.0, CH
6	119.9, CH	120.0, CH	119.7, CH	120.0, CH	119.6, CH	119.6, CH	119.7, CH
1′	198.6, C	198.8, C	204.3, C	198.7, C	204.1, C	204.4, C	203.9, C
2′	132.9, CH	132.7, CH	37.5, CH_2	132.8, CH	46.4, CH_2	47.1, CH_2	45.3, CH_2
3′	146.0, C	146.4, C	127.7, C	146.6, C	82.0, C	81.6, C	82.1, C
4′	29.5, CH_2	29.6, CH_2	147.0, CH	29.4, CH_2	22.1, CH_2	22.5, CH_2	24.5, CH_2
5′	28.1, CH_2	27.5, CH_2	27.3, CH_2	27.3, CH_2	38.4, CH_2	37.6, CH_2	36.2, CH_2
6′	127.6, CH	31.6, CH_2	31.7, CH_2	31.9, CH_2	32.5, CH_2	36.7, CH_2	126.0, CH
7′	140.3, C	40.7, CH	37.8, CH	37.5, CH	41.4, CH	42.1, CH	140.8, C
8′	35.0, CH_2	31.3, CH_2	31.0, CH_2	31.6, CH_2	36.4, CH_2	32.7, CH_2	36.5, CH_2
9′	27.2, CH_2	25.9, CH_2	25.8, CH_2	25.7, CH_2	26.3, CH_2	26.2, CH_2	27.4, CH_2
10′	130.2, CH	130.8, CH	130.1, CH	130.3, CH	130.5, CH	130.4, CH	129.5,CH
11′	131.5, C	131.5, C	132.0, C	131.9, C	131.2, C	131.7, C	132.0, C
12′	71.1, CH_2	71.2, CH_2	71.0, CH_2	71.0, CH_2	71.1, CH_2	71.1, CH_2	70.9, CH_2
13′	14.1, CH_3	14.1, CH_3	14.1, CH_3	14.1, CH_3	14.0, CH_3	14.1, CH_3	14.1, CH_3
14′	172.7, C	170.0, C	170.4, C	169.9, C	178.0, C	178.2, C	177.1, C
15′	59.9, CH_2	65.4, CH_2	67.5, CH_2	67.9, CH_2	69.2, CH_2	70.9, CH_2	66.8, CH_2
16′			173.0, C	173.2, C			
17′			20.7, CH_3	20.8, CH_3			
1″	169.3, C	169.3, C	169.1, C	169.2, C	169.2, C	169.3, C	169.1, C
2″	115.1, CH	115.1, CH	115.2, CH	115.1, CH	115.2, CH	115.1, CH	115.1, CH
3″	146.6, CH	146.9, CH	146.6, CH	146.6, CH	146.5, CH	146.6, CH	146.6, CH
4″	127.1, C	127.7, C	127.1, C	127.1, C	127.1, C	127.1, C	127.1, C
5″	131.2, CH	115.1, CH	131.2, CH	131.2, CH	131.2, CH	131.2, CH	131.2, CH
6″	116.8, CH	146.8, C	116.8, CH	116.8, CH	116.8, CH	116.8, CH	116.8, CH
7″	161.1, C	149.6, C	161.2, C	161.2, C	161.3, C	161.2, C	161.3, C
8″	116.8, CH	116.5, CH	116.8, CH	116.8, CH	116.8, CH	116.8, CH	116.8, CH
9″	131.2, CH	123.0, CH	131.2, CH	131.2, CH	131.2, CH	131.2, CH	131.2, CH

Ganoduriporol K (**6**): yellow oil; $[\alpha]_D^{25}$ +10 (*c* 0.1, MeOH); UV (MeOH) λ_{max} (log ε) 312 (4.0), 224 (4.3) nm; IR (KBr) ν_{max} (cm^{-1}): 3422, 2928, 2847, 1682, 1602, 1474, 1280, 1198 (**Figure S54**); ^1H and ^{13}C NMR data, see **Tables 1**, **2**; HRESIMS *m/z* 561.2147 $[M + Na]^+$ (calcd for $C_{30}H_{34}NaO_9$, 561.2095).

Ganoduriporol L (**7**): yellow oil; $[\alpha]_D^{25}$ +14 (*c* 0.1, MeOH); UV (MeOH) λ_{max} (log ε) 299 (4.4), 263 (4.1) nm; IR (KBr) ν_{max} (cm^{-1}): 3418, 2928, 1693, 1602, 1512, 1391, 1170 (**Figure S63**); ^1H and ^{13}C NMR data, see **Tables 1**, **2**; HRESIMS *m/z* 559.1918 $[M + Na]^+$ (calcd for $C_{30}H_{32}NaO_9$, 559.1939).

PTP1B Inhibition Assay

The expressed and purified methods of recombinant PTP1B catalytic domain were the same as references (Liu et al., 2018). The dephosphorylation of *p*-nitrophenyl phosphate (*p*NPP) generated the product pNP, which can be monitored at an absorbance for 405 nm. The compounds were pre-incubated with the enzyme at 37 °C for 5 min. Assay was performed in the final volume of 100 μL in the active system containing 50 μL reaction buffer, 25.5 μL double distilled water, 2 μL test compounds and 10 μL enzymes. After incubation at 37°C for 15 min, the reaction was terminated using 0.5 M *p*NPP (12.5 μL). After initializing the enzymatic reaction, the plate was then read every 20 s for 15 min in the microplate reader at 405 nm. Sodium orthovanadate (Na_3VO_4) was used as a positive control. The equation used was: $[(A_{blank}\text{-}A_{sample})/A_{blank}] \times 100\%$. The IC_{50} values were determined by linear or non-linear regression analysis of the concentration-response data curve.

Cytotoxicity Assay

All isolated compounds **1**-**7** were evaluated for their cytotoxicity against BEL, K562, SGC7901, A549 and Hela cell lines. The cytotoxic activities were assayed by using the MTT method in 96 well plates according to the previous report (Shi et al., 2008).

TABLE 2 | ^{1}H NMR (500 MHz) Data of Compounds **1-7** in CD_3OD (δ in ppm, J in Hz).

NO.	1	2	3	4	5	6	7
3	7.13, d (2.9)	7.11, d (2.7)	7.34, d (2.8)	7.09, d (2.7)	7.25, d (3.0)	7.29, d (2.8)	7.23, d (2.9)
5	7.05,dd (9.0, 2.9)	7.01, dd (8.9, 2.7)	6.99, dd (8.9, 2.8)	7.09, dd (8.9, 2.7)	6.99, dd (8.9, 3.0)	7.04, dd (8.9, 2.8)	6.98, dd (9.0, 2.9)
6	6.84, d (9.0)	6.80, d (8.9)	6.78, d (8.9)	6.79, d (8.9)	6.77, d (8.9)	6.80, d (8.9)	6.75, d (9.0)
2′	7.70, s	7.65, s	4.06, s	7.64, s	3.64, m 3.30, overlap	3.73, overlap 3.24, m 3.24 (m)	3.77, m 3.33, m
4′	2.65, t (7.5)	2.54, t (7.5)	2.22, t (7.7)	2.52, t (7.5)	1.75, overlap 1.57, m	1.79, m 1.72, m	2.28, overlap 2.21, m
5′	2.31, m	1.51, m	2.22, m	1.58, m	2.19, m 2.03, overlap	2.13, m	2.28, overlap 2.17, m
6′	5.26, t (7.7)	1.39, overlap 1.27, overlap	1.49, overlap 1.38, overlap	1.31, m	1.33, m 1.21, overlap	1.87, m 1.14, m	5.43, overlap
7′		1.39, overlap	1.68, m	1.50, m	1.68, m	1.61, m	
8′	2.07, overlap	1.39, overlap 1.27, overlap	1.49, overlap 1.38, overlap	1.31, m	1.74, overlap 1.21, overlap	1.31, m 1.24, m	1.96, overlap
9′	2.10, overlap	2.03, m	2.08, m	2.03, m	2.03, overlap	2.09, m	2.10, m 1.97, overlap
10′	5.43, t (6.7)	5.45, t (7.2)	5.44, t (7.3)	5.43, t (7.2)	5.46, t (7.3)	5.50, t (7.3)	5.43, overlap
12′	4.53, s	4.51, s	4.52, s	4.50, s	4.53, s	4.57, s	4.53, s
13′	1.65, s	1.65, s	1.65, s	1.64, s	1.63, s	1.69, s	1.65, s
15′	4.07, s	3.41, m	4.00, m	3.93, m	3.59, m	3.73, overlap 3.55, m	4.23, m 4.17, m
17′			1.96, s	1.96, s			
2″	6.31, d (15.9)	6.23, d (16.0)	6.31, d (15.9)	6.28, d (15.8)	6.32, d (16.0)	6.35, d (16.0)	6.31, d (15.9)
3″	7.60, d (15.9)	7.49, d (16.0)	7.58, d (15.9)	7.55, d (15.8)	7.59, d (16.0)	7.62, d (16.0)	7.58, d (15.9)
5″	7.44, d (8.4)	7.01, s	7.43, d (8.3)	7.40, d (8.1)	7.44, d (8.5)	7.48, d (8.6)	7.42, d (8.5)
6″	6.80, d (8.4)		6.78, d (8.3)	6.74, d (8.1)	6.79, d (8.5)	6.83, d (8.6)	6.77, d (8.5)
8″	6.80, d (8.4)	6.78, d (8.3)	6.78, d (8.3)	6.74, d (8.1)	6.79, d (8.5)	6.83, d (8.6)	6.77, d (8.5)
9″	7.44, d (8.4)	6.90, d (8.3)	7.43, d (8.3)	7.40, d (8.1)	7.44, d (8.5)	7.48, d (8.6)	7.42, d (8.5)

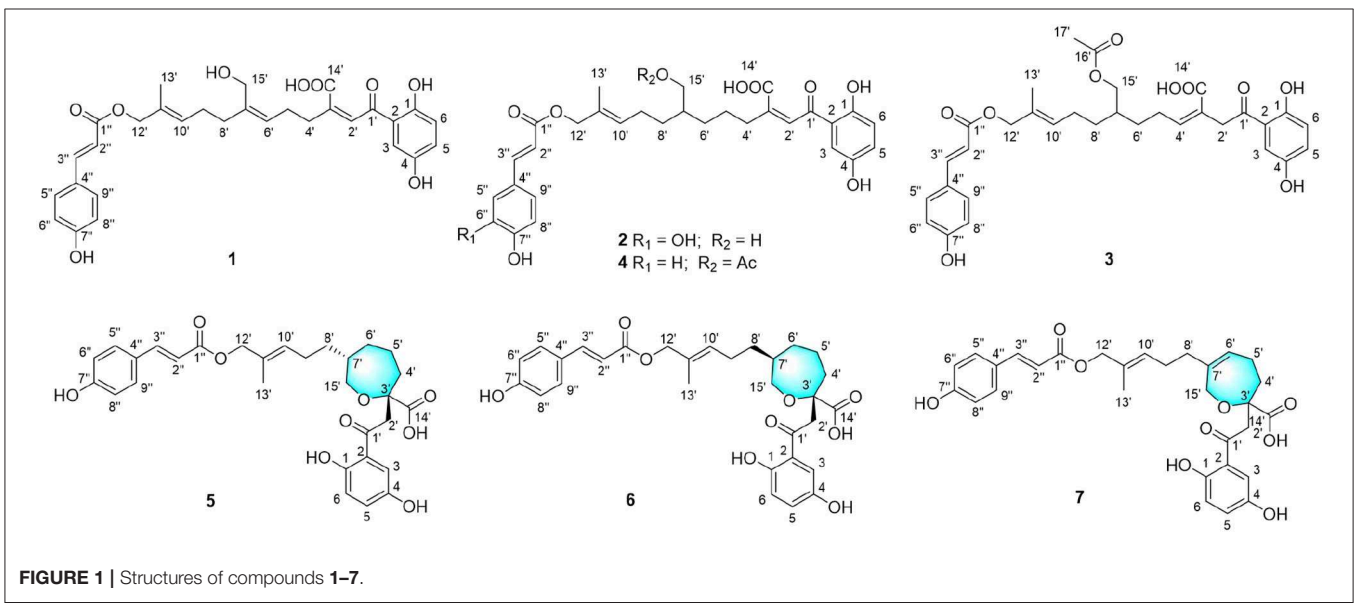

FIGURE 1 | Structures of compounds **1–7**.

Molecular Docking

Docking simulation referred to the published literature (Zhang et al., 2017). It was carried out by means of the SYBYL-X 2.0 software. All the ligand molecular were drawn using the standard parameters of SYBYL-X, then their geometric conformations were energy minimized employing the Tripos force field for 1,000

steps and Gasteiger-Huckel charges were calculated. Protein receptor (**PDB: 1QXK**) was prepared using the standard way. The H-bonds were shown using dotted line. Pymol was used as a viewer for interaction between ligands and protein receptor.

RESULTS AND DISCUSSION

Identification of Compounds 1-7

Compound **1** was obtained as yellow oil, with a molecular formula of $C_{30}H_{32}O_9$ from the molecular ion peak $[M + Na]^+$ at *m/z* 559.1938 (calcd 559.1939) in the HRESIMS (**Figure S8**). The ^{1}H NMR revealed diagnostic signals of a 2-substituted-1,4-dihydroxylbenzene moiety (δ_H 7.13, 7.05, and 6.84), a *p*-substituted hydroxybenzene substructure (δ_H 7.44 and 6.80), three olefinic singlets (δ_H 7.70, 5.26, and 5.43), two conjugated olefinic doublets (δ_H 6.31 and 7.60), and one methyl (δ_H 1.65). The ^{13}C NMR and the DEPT spectra (**Table 1**, **Figures S2, S3**) showed a total of 30 carbon signals including one methyl, six methylenes with two oxygenated, twelve sp^2 methines, and eleven sp^2 quaternary carbons including three carboxylic or carbonyl carbons. Comparison of its ^{1}H and ^{13}C NMR spectral data (**Tables 1**, **2**, **Figures S1–S6**) with those of ganoduriporol A (Chen et al., 2017) suggested that **1** had a similar structure to ganoduriporol A. Their main structural difference was that the $CH_2 - 2'$/CH-3′ substructure in ganoduriporol A was dehydrogenated to form an tri-substituted double bond in **1**, as suggested by heteronuclear multiple bond coherence spectroscopy (HMBC) correlations from the olefinic proton H-2′ (δ_H 7.70) to C-3′ (δ_C 146.0), C-4′ (δ_C 29.5), and C-1′ (δ_C 198.6). The configurations of the double bonds as 2′*Z*, 6′*Z*, 10′*E*, and 2″*E* were supported by rotating frame overhauser effect spectroscopy (ROESY) correlations (**Figures 1**, **2**, **Figure S7**) of H-2′/H_2-4′ (δ_H 2.65), H-6′ (δ_H 5.26)/H_2-8′ (δ_H 2.07), H-10′ (δ_H 5.43)/H_2-12′ (δ_H 4.53), and H-2″ (δ_H 6.31)/H-9″ (δ_H 7.44), respectively.

Compound **2** was obtained as yellow oil with a molecular formula of $C_{30}H_{34}O_{10}$ according to the HRESIMS data (**Figure S17**). Comparison of the NMR data (**Tables 1**, **2**, **Figures S10–S15**) of **2** with those of **1** revealed the presence of an additional hydroxyl at C-6″ (δ_C 146.8) in **2**, which was further confirmed by the HMBC correlations of H-5″ (δ_H 7.01) and H-8″ (δ_H 6.78) to C-6″ (δ_C 146.8). Besides, the presence of CH_2-6′/CH-7′ fragment in **2** instead of olefinic double bond CH-6′/C-7′ as in **1** was revealed by HMBC correlations from H_2-15′ (δ_H 3.41) to C-6′ (δ_C 31.6), C-7′ (δ_C 40.7), and C-8′ (δ_C 31.3) (**Figures 1**, **2**). The configurations of 2′*Z*, 10′*E* and 2″*E* in compound **2** were revealed by ROESY correlations (**Figure 2**, **Figure S16**) of H-2′ (δ_H 7.65)/H_2-4′ (δ_H 2.54), H-10′ (δ_H 5.45)/H_2-12′ (δ_H 4.51), and H-2″ (δ_H 6.23)/H-5″.

Compound **3** was obtained as yellow oil, and its molecular formula $C_{32}H_{36}O_{10}$ was concluded from the HRESIMS (**Figure S26**) *m/z* 603.2212 ($[M + Na]^+$, calcd 603.2201), implying 15 degrees of unsaturation. Its ^{1}H NMR and ^{13}C NMR data (**Tables 1**, **2**, **Figures S19–S24**) were very similar to those of ganoduriporol B (Chen et al., 2017) with the main difference being the presence of signals for an acetyl group, which located at C-15′ (δ_C 67.5) as suggested by HMBC correlations (**Figures 1**, **2**) from H_2-15′ (δ_H 4.00) and a singlet methyl proton signal at δ_H 4.00 to the ester carbonyl at δ_C 173.0. Besides, the CH-3′/CH_2-4′ substructure in ganoduriporol B was dehydrogenated to afford an olefinic C-3′/CH-4′ double bond in **3**, as revealed by HMBC correlations from $H_2 - 2'$ (δ_H 4.06) to C-1′ (δ_C 204.3), C-3′ (δ_C 127.7), C-4′ (δ_C 147.0), and C-14′ (δ_C 170.4). The configurations of 3′*Z*, 10′*E* and 2″*E* in compound **3** were revealed by the ROESY correlations (**Figure 2**, **Figure S25**) of $H_2 - 2'$/H-4′ (δ_H 2.22), H-10′ (δ_H 5.44)/H_2-12′ (δ_H 4.52), and H-2″ (δ_H 6.31)/H-5″ (δ_H 7.43).

Compound **4** was isolated as yellow oil. Its molecular formula was determined as $C_{32}H_{36}O_{10}$ by HRESIMS (**Figure S35**), the same as that of **3**. The NMR data of **4** were quite similar to those of **3** (**Tables 1**, **2**). Analysis of the 2D NMR data (**Figure 2**, **Figures S28–S33**) of **4** suggested their only structural difference was the position of one double bond, which was located C-2′ (δ_C 132.8) and C-3′ (δ_C 146.6) in **4** instead of at C-3′ (δ_C 127.7) and C-4′ (δ_C 147.0) as in **3**, as confirmed by HMBC correlations from the olefinic proton H-2′ (δ_H 7.64) to C-3′ (δ_C 146.6), C-4′ (δ_C 29.4), and C-1′ (δ_C 198.7). The configurations of 2′*Z*, 10′*E*, and 2″*E* in compound **4** were elucidated by ROESY correlations (**Figures 1**, **2**, **Figure S34**) of H-2′/H_2-4′ (δ_H 2.52), H-10′ (δ_H 5.43)/H_2-12′ (δ_H 4.50), and H-2″ (δ_H 6.28)/H-9″ (δ_H 7.40).

Compound **5** was assigned the molecular formula as $C_{30}H_{34}O_9$ on the basis of HRESIMS data (**Figure S44**), indicating 14 degrees of unsaturation. The ^{1}H NMR and ^{13}C NMR, together with ^{1}H-detected heteronuclear single quantum coherence spectrum (HSQC), revealed the presence of one methyl, eight methylenes (two oxygenated), eleven methines, and ten quaternary carbons. Comparison of NMR data (**Figures S37–S42**) between compounds **5** and **1** found that the $\Delta^{2'}$ double bond in **1** was replaced by a methylene ($\delta_{C/H}$ 69.2/3.59) and an oxygenated quaternary carbon (δ_C 82.0), the latter of which was linked to C-2′ (δ_C 46.4) via an oxygen atom to form an oxepane rings, as suggested by HMBC correlations from $H_2 - 2'$ (δ_H 3.64) to C-3′ (δ_C 82.0), C-14′ (δ_C 178.0), and C-1′ (δ_C 204.1) and from H_2-15′ (δ_H 3.59) to C-3′. The other difference was that the double bond at C-6′ (δ_C 127.6) and C-7′ (δ_C 140.3) in **1** was replaced by a sp^3 methine and methylene in **5**, as confirmed by COSY correlations (**Figures 1**, **2**) of H-7′ (δ_H 1.68) with H_2-6′ (δ_H 1.21), H_2-8′ (δ_H 1.74) and H_2-15′. The *E* configurations of $\Delta^{10'}$ and $\Delta^{2''}$ double bonds were established by the ROESY correlations (**Figure 2**, **Figure S43**) from H-10′ (δ_H 5.46) to H_2-12′ (δ_H 4.53) and the coupling constant ($J = 16.0$ Hz) between H-2″ (δ_H 6.32) and H-3″ (δ_H 7.59), respectively. ROESY correlations from $H_2 - 2'$ (δ_H 3.64)/H-7′ (δ_H 1.68) suggested that $CH_2 - 2'$ and CH_2-8′ were on the face opposite to each other.

Compound **6** was determined to have a molecular formula $C_{30}H_{34}O_9$ based on HRESIMS (**Figure S53**) analysis, the same as that of **5**. The 1D NMR data of **6** were almost identical to those of **5**. Analysis of the 2D NMR data (**Figures S46–S51**) of **6** found that compounds **5** and **6** shared the same planar

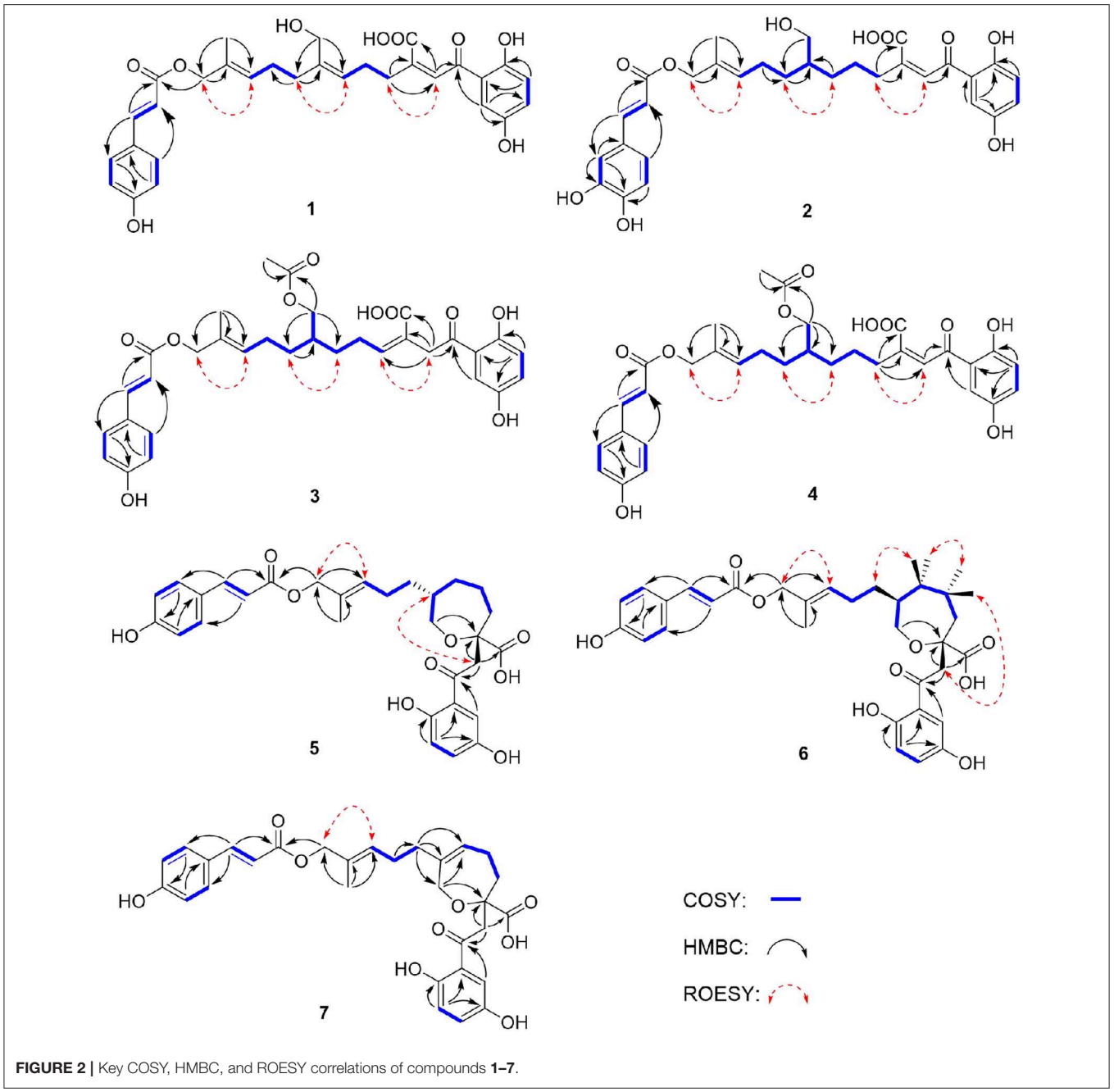

FIGURE 2 | Key COSY, HMBC, and ROESY correlations of compounds **1–7**.

structure, indicating that they are a pair of stereoisomers. The *E* configuration of $\Delta^{10'}$ and $\Delta^{2''}$ double bonds were established by the ROESY correlations (**Figures 1**, **2**, **Figure S52**) from H-10′ (δ_H 5.50) to H_2-12' (δ_H 4.57) and the coupling constant (J = 16.0 Hz) between H-2″ (δ_H 6.35) and H-3″ (δ_H 7.62), respectively. ROESY correlations from H_2-2' (δ_H 3.24)/H_2-4′α (δ_H 1.72), and H_2-4′β (δ_H 1.79)/$H_2-6'\beta$ (δ_H 1.14), and H_2-6′α (δ_H 1.87)/H_2-8′α (δ_H 1.31) suggested that CH_2-2' and CH_2-8' were on the same face of the ring system, which is different with that of **5**.

Compound **7** was obtained as a yellow oil with a molecular ion peak at *m/z* 559.1938 $[M + Na]^+$ in HRESIMS (**Figure S62**), coinciding with the molecular formula $C_{30}H_{32}O_9$. Comparison of the NMR data (**Figures S55–S60**) revealed that the structure of **7** was very similar to that of **5**, with the difference being the CH_2 (6′)-CH (7′) substructure in **5** was replaced by a tri-substituted double bond CH (6′)-C (7′) in **7**, which was deduced from the HMBC correlations from H_2-8′ (δ_H 1.96) to C-6′ (δ_C 126.0) and C-7′ (δ_C 140.8). The configurations of 6′*Z*, 10′*E*, and 2″*E* in compound **7** were elucidated by ROESY correlations

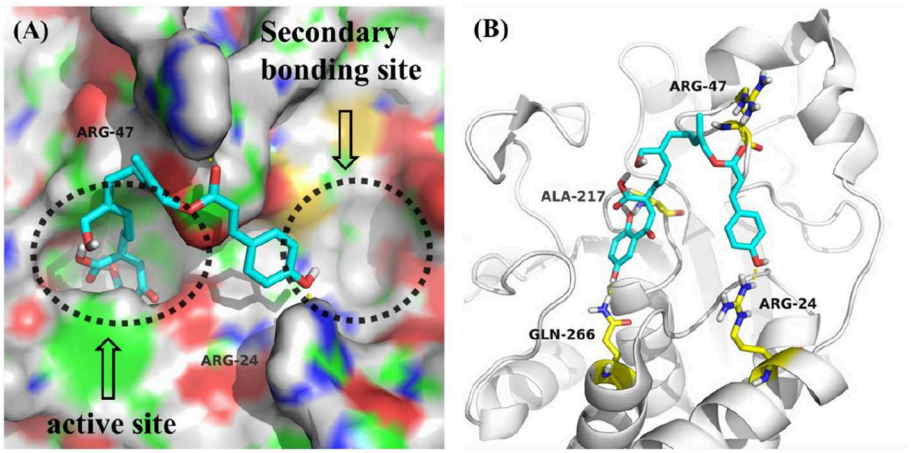

FIGURE 3 | (A) Model of compound **1** (cyans) bound to PTP1B (PDB: 1QXK). **(B)** Interactions between compound **1** (cyans) and PTP1B. The key amino acids were shown in yellow.

(**Figure S61**) of H_2-8′ (δ_H 1.96)/H-6′ (δ_H 5.43), H-10′ (δ_H 5.43)/H_2-12′ (δ_H 4.53), and H-2″ (δ_H 6.31)/H-9″ (δ_H 7.42).

All compounds isolated were evaluated for their inhibitory activities against PTP1B using *p*NPP as a substrate and cytotoxicities against BEL, K562, SGC7901, A549, and Hela human cell lines using the MTT method. All of the compounds were non-cytotoxic against the tested tumor cell lines. Compounds **1**-**4** showed obvious inhibitory activity against PTP1B with IC_{50} values of 17, 20, 19, and 23 μM (**Figure S64**), respectively, comparable to the positive control Na_3VO_4 (IC_{50} = 12 μM). A positive effort was made to explain the activity of compound **1** against PTP1B by performing molecular docking (**Figure 3**). Docking results implied that **1** binds deep in the active site pocket and form H-bonds with ALA-217 and GLN-266, and the 7″-OH also formed H-bond with ARG-24 which was located in the so-called secondary binding site of PTP1B. Thus, it is a potent active molecule against PTP1B, with the ability to interact with both bonding sites. Based on the above research, we believed that it was feasible and reasonable to obtain PTP1B inhibitors with medicinal potential through appropriate structural modifications of these compounds. The cytotoxicity assessment also further provided evidence for this idea, for that all the compounds were inactive against the tested tumor cell lines.

CONCLUSIONS

In summary, seven new meroterpenoids were isolated and identified from the fruiting bodies of *G. ahmadii*. Among them, compounds **1**–**4** exhibited inhibitory activity against PTP1B but no cytotoxicity against the tested five tumor cell lines, suggesting that it has great potential to obtain new PTP1B inhibitors with medicinal use through appropriate structural modifications of these compounds. The possible mechanisms of these compounds against PTP1B were also revealed by molecular docking experiment. These findings once again proved the great medicinal values of *Ganoderma* fungi.

DATA AVAILABILITY STATEMENT

All datasets generated for this study are included in the article/**Supplementary Material**.

AUTHOR CONTRIBUTIONS

JG and FK performed the experiments. QM contributed to the bioassays. QX collected the fruiting bodies of *G. ahmadii*. RZ was responsible for edited pictures. YZ and YW designed the work and revised the paper. All authors have approved the final version of the manuscript.

ACKNOWLEDGMENTS

This work was supported by Natural Science Foundation of Hainan Province (219MS078), Natural Science Foundation of China (81973568), China Agriculture Research System (CARS-21), and Central Public-interest Scientific Institution Basal Research Fund for Chinese Academy of Tropical Agricultural Sciences (17CXTD-15, 1630052016008).

SUPPLEMENTARY MATERIAL

The Supplementary Material for this article can be found online at: https://www.frontiersin.org/articles/10.3389/fchem.2020.00279/full#supplementary-material

REFERENCES

Baby, S., Johnson, A. J., and Govindan, B. (2015). Secondary metabolites from *Ganoderma*. *Phytochemistry* 114, 66–101. doi: 10.1016/j.phytochem.2015.03.010

Cai, J. Y., Zhao, L., and Tao, W. (2015). Potent protein tyrosine phosphatase 1B (PTP1B) inhibiting constituents from *Anoectochilus chapaensis* and moleculardocking studies. *Pharm. Biol.* 53, 1030–1034. doi: 10.3109/13880209.2014.957781

Chen, C., Liang, F., Chen, B., Sun, Z. Y., Xue, T. D., Yang, R. L., et al. (2017). Identifification of demethylincisterol A_3 as a selective inhibitor of protein tyrosine phosphatase Shp2. *Eur. J. Pharmacol.* 795, 124–133. doi: 10.1016/j.ejphar.2016.12.012

Fu, Y. L., Shi, L., and Ding, K. (2019). Structure elucidation and anti-tumor activity *in vivo* of a polysaccharide from spores of *Ganoderma lucidum* (Fr.) Karst. *Int. J. Biol. Macromol.* 141, 693–699. doi: 10.1016/j.ijbiomac.2019.09.046

Guo, J. C., Ma, Q. Y., Kong, F. D., Xie, J. Y., Zhou, L. M., Ding, Q., et al. (2019). Meroterpenoids from the fruiting bodies of *Ganoderma ahmadii* Steyaret and their PTP1B inhibitory activities. *Chin. J. Org. Chem.* 39, 3264–3268. doi: 10.6023/cjoc201905010

Huang, C. Y., Chen, J. Y. F., Wu, J. E., Pu, Y. E., Liu, G. Y., Pan, M. H., et al. (2010). Ling-Zhi polysaccharides potentiate cytotoxic effects of anticancer drugs against drug-resistant urothelial carcinoma cells. *J. Agric. Food. Chem.* 58, 8798–8805. doi: 10.1021/jf1020158

Huang, S. Z., Cheng, B. H., Ma, Q. Y., Wang, Q., Kong, F. D., Dai, H. F., et al. (2016). Anti-allergic prenylated hydroquinonesand alkaloids from the fruiting body of *Ganoderma calidophilum*. *RSC. Adv.* 6, 21139–21147. doi: 10.1039/C6RA01466F

Huang, S. Z., Ma, Q. Y., Kong, F. D., Guo, Z. K., Cai, C. H., Hu, L. L., et al. (2017). Lanostane-type triterpenoids from the fruiting body of *Ganoderma calidophilum*. *Phytochemistry* 143, 104–110. doi: 10.1016/j.phytochem.2017.07.015

Ji, Z., Tang, Q. J., Zhang, J. S., Yang, Y., Jia, W., and Pan, Y. J. (2007). Immunomodulation of RAW264.7 macrophages by GLIS, a proteopolysaccharide from *Ganoderma lucidum*. *J. Ethnopharmacol.* 112, 445–450. doi: 10.1016/j.jep.2007.03.035

Li, K., Na, K., Sang, T. T., Wu, K. K., Wang, Y., and Wang, X. Y. (2017). The ethanol extracts of sporoderm-broken spores of *Ganoderma lucidum* inhibit colorectal cancer *in vitro* and *in vivo*. *Oncol. Rep.* 38, 2803–2813. doi: 10.3892/or.2017.6010

Liu, J. Q., Lian, C. L., Hu, T. Y., Wang, C. F., Xu, Y., Xiao, L., et al. (2018). Two new farnesyl phenolic compounds with anti-inflammatory activities from *Ganoderma duripora*. *Food. Chem.* 263, 155–162. doi: 10.1016/j.foodchem.2018.04.097

Lu, S. Y., Peng, X. R., Dong, J. R., Yan, H., Kong, Q. H., Shi, Q. Q., et al. (2019). Aromatic constituents from *Ganoderma lucidum* and their neuroprotective and anti-inflammatory activities. *Fitoterapia* 134, 58–64. doi: 10.1016/j.fitote.2019.01.013

Ma, L. F., Yan, J. J., Lang, H. Y., Jin, L. C., Qiu, F. J., Wang, Y. J., et al. (2019). Bioassay-guided isolation of lanostane-type triterpenoids as α-glucosidase inhibitors from *Ganoderma hainanense*. *Phytochem. Lett.* 29, 154–159. doi: 10.1016/j.phytol.2018.12.007

Paterson, R. R. M. (2006). *Ganoderma*-a therapeutic fungal biofactory. *Phytochemistry* 67, 1985–2001. doi: 10.1016/j.phytochem.2006.07.004

Qiu, J., Wang, X., and Song,. C. (2016). Neuroprotective and antioxidant lanostanoid triterpenes from the fruiting bodies of *Ganoderma atrum*. *Fitoterapia* 109, 75–79. doi: 10.1016/j.fitote.2015.12.008

Shi, L., Yu, H. P., Zhou, Y. Y., Du, J. Q., Shen, Q., Li, J. Y., et al. (2008). Discovery of a novel competitive inhibitor of PTP1B by high-throughput screening. *Acta. Pharmacol. Sin.* 29, 278–284. doi: 10.1111/j.1745-7254.2008.00737.x

Tamrakar, A. K., Maurya, C. K., and Rai, A. K. (2014). PTP1B inhibitors for type 2 diabetes treatment: a patent review (2011-2014). *Expert. Opin. Ther. Pat.* 24, 1101–1115. doi: 10.1517/13543776.2014.947268

Teng, B. S., Wang, C. D., Yang, H. J., Wu, J. S., Zhang, D., Zhang, D., et al. (2011). A protein tyrosine phosphatase 1B activity inhibitor from the fruiting bodies of *Ganoderma lucidum* (Fr.) karst and its hypoglycemic potency on streptozotocin-induced type 2 diabetic mice. *J. Agric. Food. Chem.* 59, 6492–6500. doi: 10.1021/jf200527y

Wang, C. H., Hsieh, S. C., Wang, H. J., Chen, M. L., Lin, B. F., Chiang, B. H., et al. (2014). Concentration variation and molecular characteristics of soluble (1,3;1,6)-β-D-glucans in submerged cultivation products of *Ganoderma lucidum* mycelium. *J. Agric. Food. Chem.* 62, 634–641. doi: 10.1021/jf404533b

Wang, K., Bao, L., Ma, K., Zhang, J., Chen, B., Han, J., et al. (2017). A novel class of α-glucosidase and HMG-CoA reductase inhibitors from *Ganoderma leucocontextum* and the anti-diabetic properties of ganomycin I in KK-A^y mice. *Eur. J. Med. Chem.* 127, 1035–1046. doi: 10.1016/j.ejmech.2016.11.015

Wang, L. J., Jiang, B., Wu, N., Wang, S. Y., and Shi, D. Y. (2015). Small molecules as potent protein tyrosine phosphatase 1B (PTP1B) inhibitors documented in patents from 2009 to 2013. *Mini. Rev. Med. Chem.* 15, 104–122. doi: 10.2174/1389557515666150203144339

Wu, X. L., and Dai, Y. C. (2005). *Coloured Illustartions of Ganodermatacete of China*. Beijing: Science Press.

Yan, Y. M., Ai, J., Zhou, L. L., Chung, A. C. K., Li, R., Nie, J., et al. (2013). Lingzhiols, unprecedented rotary door-shaped meroterpenoids as potent and selective inhibitors of p-Smad3 from *Ganoderma lucidum*. *Org. Lett.* 15, 5488–5491. doi: 10.1021/ol4026364

Zhang, R., Yu, R., Xu, Q., Li, X., Luo, J., Jiang, B., et al. (2017). Discovery and evaluation of the hybrid of bromophenol and saccharide as potent and selective protein tyrosine phosphatase 1B inhibitors. *Eur. J. Med. Chem.* 134, 24–33. doi: 10.1016/j.ejmech.2017.04.004

Zhang, S. S., Wang, Y. G., Huang, S. Z., Hu, L. L., Dai, H. F., Yu, Z. F., et al. (2015). Three new lanostanoids from the mushroom *Ganoderma tropicum*. *Molecules* 20, 3281–3289. doi: 10.3390/molecules20023281

Zhao, R. L., and He, Y. M. (2018). Network pharmacology analysis of the anti-cancer pharmacological mechanisms of *Ganoderma lucidum* extract with experimental support using Hepa1-6-bearing C57 BL/6 mice. *J. Ethnopharmacol.* 210, 287–295. doi: 10.1016/j.jep.2017.08.041

Zhao, Z. Z., Chen, H. P., Feng, T., Li, Z. H., Dong, Z. J., and Liu, J. K. (2015). Lucidimine A-D, four new alkaloids from the fruiting bodies of *Ganoderma lucidum*. *J. Asian Nat. Prod. Res.* 17, 1160–1165. doi: 10.1080/10286020.2015.1119128

Conflict of Interest: The authors declare that the research was conducted in the absence of any commercial or financial relationships that could be construed as a potential conflict of interest.